(e.g., *Dictyostelium*, fungi, and plants), apparently lack many proteins used by animals for signaling and adhesion. Therefore, choanoflagellates, with their closer evolutionary relationship to animals (*4*–*7*) and their expression of signaling and cell adhesion protein homologs, are more informative for studies of animal origins.

The existence in unicellular choanoflagellates of proteins used for cell adhesion and signal transduction in animals prompts the question of their ancestral function in the progenitor of animals and choanoflagellates. Despite the apparent simplicity of the choanoflagellate lifestyle, it is possible that choanoflagellate homologs of animal proteins perform similar biochemical functions within a unicellular context. For instance, TKs may act in choanoflagellates to detect changes in the extracellular environment, as we have demonstrated through their response to nutrient availability. In addition, animal cell adhesion proteins, such as the cadherins, may derive from ancestral proteins that stabilized the interactions between protozoan cells during conjugation or colony formation. Proteins that mediate cell attachment or defense against pathogens in animals may have evolved from proteins required for prey recognition and capture. C-type lectins might allow choanoflagellates to distinguish between and capture different bacterial species by binding specific sugar groups displayed on bacterial cell walls. Targeted manipulations of gene function in choanoflagellates will be necessary to test hypotheses about the ancestral roles of these conserved molecules.

We have sampled just a fraction of the choanoflagellate proteome. The diversity of choanoflagellate proteins predicted to function in cell interactions suggests that additional proteins shared exclusively with animals will be discovered through sequencing the entire choanoflagellate genome. Of particular interest will be the repertoire of transcription factors and the potential representation of families of proteins that regulate cell differentiation and development in animals. It may then be possible to determine whether entire regulatory pathways linking receptor-based signaling inputs to gene regulation and cell behavior predate the origin of animals.

References and Notes

1. Comparisons of yeast, *Caenorhabditis*, *Drosophila*, and human genomes have revealed a set of protein domains conserved among Bilateria and absent from yeast (*25*, *26*). However, because the Bilateria represent a recent derivation within the Metazoa and the Fungi diverged from the animal lineage long before the transition to multicellularity, comparisons limited to fungal and bilaterian animal genomes do not reveal the complexity of the ancestral animal genome.
2. W. Saville Kent, *A Manual of the Infusoria* (David Bogue, London, 1880–1882).
3. D. J. Hibberd, *J. Cell Sci.* **17**, 191 (1975).
4. P. O. Wainright, G. Hinkle, M. L. Sogin, S. K. Stickel, *Science* **260**, 340 (1993).
5. N. King, S. B. Carroll, *Proc. Natl. Acad. Sci. U.S.A.* **98**, 15032 (2001).
6. E. A. Snell, R. F. Furlong, P. W. H. Holland, *Curr. Biol.* **11**, 967 (2001).
7. B. F. Lang, C. O'Kelly, T. Nerad, M. W. Gray, G. Burger, *Curr. Biol.* **12**, 1773 (2002).
8. G. Burger, L. Forget, Y. Zhu, M. W. Gray, B. F. Lang, *Proc. Natl. Acad. Sci. U.S.A.* **100**, 892 (2003).
9. R. F. Watkins, A. T. Beckenbach, *J. Mol. Evol.* **48**, 542 (1999).
10. J. L. Boore, *Nucleic Acids Res.* **27**, 1767 (1999).
11. Materials and methods are available as supporting material on *Science* Online.
12. Searchable choanoflagellate EST databases are available at http://projects.bocklabs.wisc.edu/carroll/choano/.
13. I. Letunic *et al.*, *Nucleic Acids Res.* **30**, 242 (2002).
14. A. Bateman *et al.*, *Nucleic Acids Res.* **30**, 276 (2002).
15. L. Shapiro, P. D. Kwong, A. M. Fannon, D. R. Colman, W. A. Hendrickson, *Proc. Natl. Acad. Sci. U.S.A.* **92**, 6793 (1995).
16. F. Nollet, P. Kools, F. van Roy, *J. Mol. Biol.* **299**, 551 (2000).
17. R. B. Dodd, K. Drickamer, *Glycobiology* **11**, 71R (2001).
18. X. R. Bustelo, *Mol. Cell. Biol.* **20**, 1461 (2000).
19. A. C. Porter, R. R. Vaillancourt, *Oncogene* **17**, 1343 (1998).
20. A. Levitzki, A. Gazit, *Science* **267**, 1782 (1995).
21. E. B. Pasquale, P. A. Maher, S. J. Singer, *J. Cell. Physiol.* **137**, 146 (1988).
22. K. Miyazawa *et al.*, *Blood* **80**, 1685 (1992).
23. J. A. Cooper, B. M. Sefton, T. Hunter, *Mol. Cell. Biol.* **4**, 30 (1984).
24. P. Kumar, S. Hosaka, A. E. Koch, *J. Biol. Chem.* **276**, 21039 (2001).
25. G. M. Rubin *et al.*, *Science* **287**, 2204 (2000).
26. V. Wood *et al.*, *Nature* **415**, 871 (2002).

27. We thank P. Bertics, A. Guadarrama, B. Leadbeater, and T. Hunter for advice and technical assistance; L. Olds for assistance with graphics; J. Holt for computing support; and B. Hersh and C. Malone for critical reading of the manuscript. N.K. is supported by an NIH postdoctoral fellowship (GM-20734) and C.T.H. is an HHMI predoctoral fellow. This work was supported by the HHMI (S.B.C.).

Supporting Online Material

www.sciencemag.org/cgi/content/full/301/5631/361/DC1
Materials and Methods
SOM Text
Figs. S1 to S4
Tables S1 and S2
References and Notes

25 February 2003; accepted 28 May 2003

Hox10 and *Hox11* Genes Are Required to Globally Pattern the Mammalian Skeleton

Deneen M. Wellik and Mario R. Capecchi*

Mice in which all members of the *Hox10* or *Hox11* paralogous group are disrupted provide evidence that these *Hox* genes are involved in global patterning of the axial and appendicular skeleton. In the absence of *Hox10* function, no lumbar vertebrae are formed. Instead, ribs project from all posterior vertebrae, extending caudally from the last thoracic vertebrae to beyond the sacral region. In the absence of *Hox11* function, sacral vertebrae are not formed and instead these vertebrae assume a lumbar identity. The redundancy among these paralogous family members is so great that this global aspect of *Hox* patterning is not apparent in mice that are mutant for five of the six paralogous alleles.

Hox genes have long been recognized as important transcriptional regulators of embryonic development. In mammals, this complex of 39 genes resides on four separate chromosomal linkage groups designated A, B, C, and D, which arose early in the evolution of vertebrates from successive duplications of a single ancestral complex. Homologous members within the separate linkage groups are divided into 13 sets of paralogous genes, each having two to four members. During development, paralogous sets of genes are activated sequentially, with *Hox1* and *Hox2* paralogous genes being expressed earlier and more anteriorly in the embryo and successive genes through paralogous group *Hox13* appearing later and more posteriorly.

Howard Hughes Medical Institute and University of Utah, Salt Lake City, UT 84112, USA.

*To whom correspondence should be addressed. E-mail: mario.capecchi@genetics.utah.edu

The spectrum of perturbations of the mammalian skeleton resulting from either gain- or loss-of-function mutations in individual *Hox* genes has been difficult to interpret in terms of a coherent model of how these genes participate in the patterning of the axial skeleton. Loss-of-function *Hox* mutations have yielded changes in vertebral morphology along the anteroposterior (AP) axis that have been interpreted as anterior homeotic transformations as well as posterior homeotic transformations. Typically, these morphological changes involve perturbations in one or a small number of vertebrae.

Among different vertebrate species, axial skeletal patterns have diverged considerably. A comparative survey of *Hox* gene expression in mice and chicks showed that *Hox* gene expression boundaries along the rostrocaudal axis shift in accordance with changes in the class of vertebrae produced at a given axial level (*1*). This observation suggests that *Hox* genes play a crit-

ical role in the global patterning of the vertebrate axial skeleton (*2*). Yet, over the past decade, loss-of-function studies of mice with single, and even subsets of, paralogous *Hox* gene mutations have shown, with variable expressivities and penetrance, only relatively minor changes in skeletal phenotypes, which is inconsistent with their proposed role as global regulators of axial skeletal patterning. What has complicated the analysis of *Hox* gene mutations is that these genes have retained considerable functional redundancy between paralogous groups (*3*–*9*). Therefore, we examined the effects of the loss of function of the entire group of *Hox10* and *Hox11* paralogous genes on skeletal patterning [see supporting online material for details regarding the generation of mice (*9*, *10*)].

The axial formula in mice is 7 cervical, 13 thoracic, 6 lumbar, 4 sacral, and numerous (and slightly variable numbers of) caudal vertebrae. Mice with either *Hox10* or *Hox11* paralogous mutations show drastic alterations of the axial formula. *Hox10* triple mutant skeletons completely lack lumbar vertebrae and exhibit rib processes that protrude from each vertebral segment beyond the 13th thoracic vertebra through the normal lumbar and sacral regions (compare Fig. 1, A and F). In addition to ectopic rib formation, these vertebral elements also display morphological characteristics that are normally associated with thoracic vertebrae (compare Fig. 1, B to E, with Fig. 1, G to J, and Fig. 2A with Fig. 2B). In the *Hox10* triple mutant (Fig. 1A), the severely altered sacral vertebrae still form fusions at their lateral margins to produce a pseudosacrum. This fusion occurs at the appropriate position despite the severe perturbations in morphology of these vertebral elements. Despite the changes in axial morphology, the pelvis (which also displays patterning perturbations; compare Fig. 2, D and E) and the hindlimbs associate with the pseudosacral lateral fusion at the normal position along the vertebral axis (compare Fig. 2, A and B).

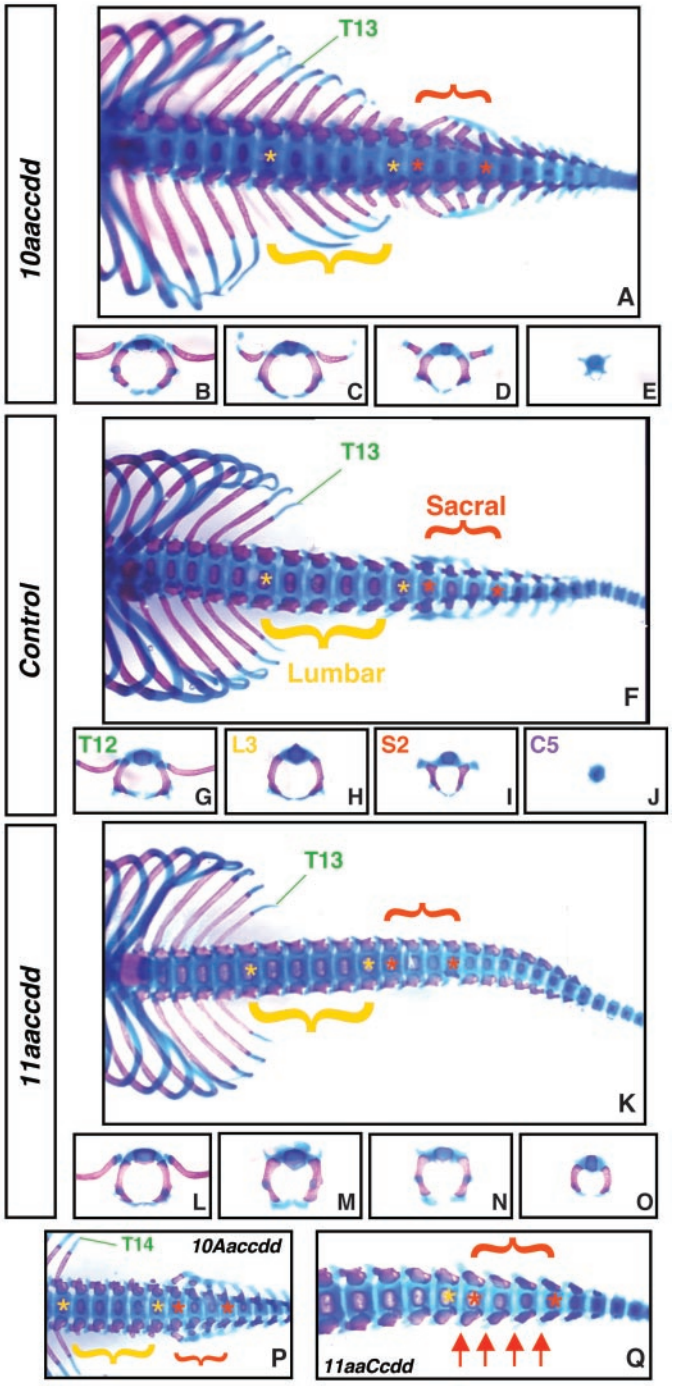

Fig. 1. Axial skeletons of *Hox10* and *Hox11* triple mutants at embryonic day 18.5 (E18.5). Ventral views of the axial skeleton from the lower thoracic region through the early caudal region of a *Hox10* triple mutant (**A**), a control (**F**), and a *Hox11* triple mutant (**K**) are shown. Yellow asterisks indicate lumbar vertebrae; red asterisks indicate sacral vertebrae. A five-allele mutant from the *Hox10* and *Hox11* paralogous mutant group is shown in (**P**) and (**Q**), respectively (red arrows indicate sacral wing formation). Analogous vertebrae were dissected from the control and from each triple mutant to compare single vertebral identities. The 19th vertebral element, normally T12, is shown in (**B**), (**G**), and (**L**). The 23rd element, normally L3, is shown in (**C**), (**H**), and (**M**). The 28th element, normally S2, is shown in (**D**), (**I**), and (**N**). The 35th element, normally caudal vertebra 5 (C5), is shown in (**E**), (**J**), and (**O**). (Between two and seven E18.5 skeletons were collected for each of the triple mutant, five-allele, and control skeletons for each paralogous group.)

Mice with only five mutant alleles display a 14th rib and altered sacral processes, but the axial morphology is much less severely affected than in the *Hox10* triple mutant (Fig. 1P). Combinations of any five of the six mutant alleles in the *Hox10* paralogous group demonstrate similar mutant phenotypes to one another, indicating the approximately equal contribution of these alleles to axial patterning (*11*). Comparison of *Hox10* five-allele mutants to *Hox10* triple mutant animals demonstrates the extent of redundancy within this paralogous group.

Hox11 triple mutant skeletons show equally severe, but distinct, axial phenotypes. Rib formation terminates normally and the lumbar vertebrae appear normal; however, no sacral vertebrae are formed. Instead, these vertebrae assume a lumbar morphology (Fig. 1K). The lumbarlike vertebral elements continue far past the normal sacral region, and caudal vertebrae are not apparent until several elements more posterior than in controls (compare Fig. 1, L to O, with Fig. 1, G to J). Mice mutant for *Hox11* paralogous genes also display severe perturbations of pelvic morphology (compare Fig. 2, F and E). However, despite the absence of sacral vertebrae in these mutants, the pelvis and hindlimbs again associate with the appropriate vertebral segments (Fig. 2C). The combined results demonstrate that the positioning of the pelvis and hindlimbs is not under the control of either *Hox10* or *Hox11* paralogous genes. Further, the AP positioning of these elements is not dependent on normal sacral development or on appropriate lumbosacral transitions.

Five-allele *Hox11* mutants again demonstrate the redundancy within the paralogous group with respect to axial phenotype. No sacral wing fusion occurs in any of the five-allele skeletons, but sacral wings do appear on more posterior elements (Fig. 1Q), and there are fewer elements that are lumbarlike posterior to the normal sacral region. It is important to note that although *Hox10* and *Hox11* triple mutants both severely affect sacral formation, these paralogs clearly perform distinct functions on the same elements. Also, even though these sets of paralogous mutations result in the complete loss

of lumbar or sacral vertebrae, the total number of vertebral elements is not altered.

The limbs of all vertebrates are composed of three basic elements: the stylopod (humerus/femur of the forelimb and hindlimb, respectively), the zeugopod (radius and ulna/tibia and fibula), and the autopod (numerous carpal, metacarpal, tarsal, metatarsal, and phalangeal elements). *HoxA* and *HoxD* complex paralogous group genes 9 to 13 are expressed and function in the developing forelimb; whereas *HoxA* and *HoxD* paralogous groups 10 to 13, as well as *Hoxc10* and *Hoxc11*, are expressed and function in the developing hindlimb (*1*, *3*, *7*, *12*–*17*). It has previously been shown that *Hoxa11/Hoxd11* and *Hoxa13/Hoxd13* play major roles in the patterning of the forelimb zeugopod and of both the forelimb and hindlimb autopod, respectively (*3, 7*). We demonstrated that *Hox10* and *Hox11* paralogous genes are required for patterning of the hindlimb stylopod and zeugopod, respectively.

In *Hox10* triple mutants, the humerus is only moderately decreased in length relative to controls, and the deltoid process is not formed (compare Fig. 3, A and B). In contrast, the formation of the femur is grossly affected in these mutants. The femur is greatly reduced in length and no patella is formed (compare Fig. 3, D and E). The *Hox10* five-allele mutants show an intermediate stylopod phenotype between wild-type and triple mutants (*11*).

Hox11 triple mutants demonstrate dramatic mispatterning of the fore- and hindlimb zeugopods (Fig. 3, C and F). The forelimb mutant phenotype is similar to that reported for *Hoxa11/Hoxd11* double mutants (*7*). However, in *Hoxa11/Hoxd11* double mutants, the formation of the tibia and fibula is only mildly affected, whereas in the *Hox11* triple mutants, the hindlimb zeugopod is grossly affected. These results are consistent with *Hoxc11* being expressed only in the hindlimbs (*12*).

The results from the genetic analysis of *Hox10* and *Hox11* paralogous genes suggest that *Hox* genes are indeed involved in global patterning of the mammalian axial skeleton. Further, one can begin to postulate mechanisms of how changes in *Hox* gene expression could account for variation of the axial formula in different vertebrate taxa. For instance, one would predict that shifts of the boundaries of *Hox10* paralogous gene expression, rostrally or caudally, would alter the number of thoracic vertebrae present in an animal. Similarly, shifts in the expression of the *Hox11* paralogous genes would predict an alteration in the position and number of sacral vertebrae. Many primitive tetrapods have ribs projecting from all vertebrae, extending from the head to the tail. This has led to the suggestion that the ground state for vertebrae includes rib projections (*18*). Our data from the mouse supports this hypothesis and provides a mechanism whereby *Hox* genes have been used during evolution to suppress and modify rib formation in the lumbosacral region. It is curious and perhaps not insignificant that the normal patterning of thoracic, lumbar, and sacral vertebrae, as well as the changes

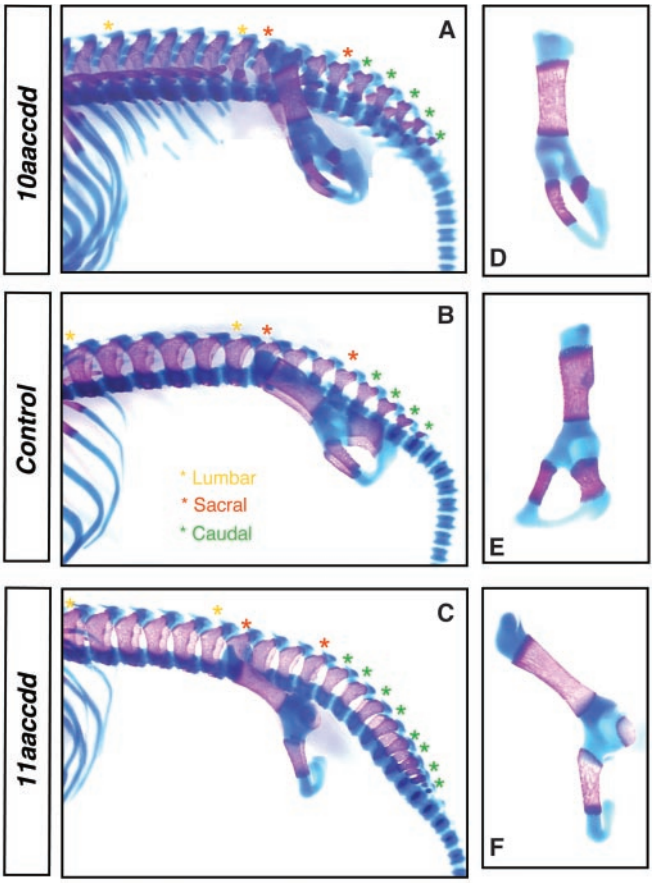

Fig. 2. Pelvic position and morphology in E18.5 *Hox10* and *Hox11* triple mutants. In (**A** to **C**), the axial skeleton associated with the pelvis is shown in lateral view from *Hox10* triple mutants, control, and *Hox11* triple mutants, respectively. Dissociated pelvic bones are shown in (**D** to **F**) for the same genotypes.

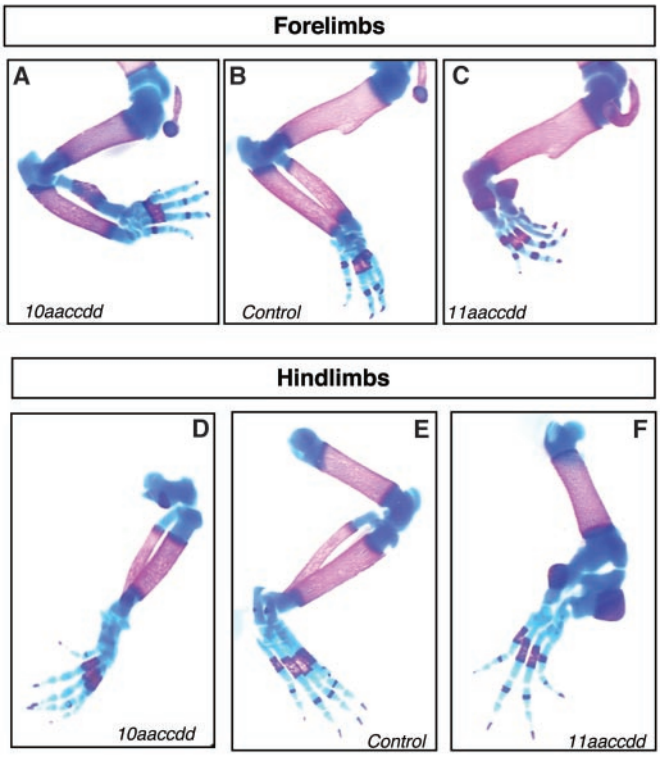

Fig. 3. Limb skeletons of E18.5 *Hox10* and *Hox11* triple mutant mice. (**A** and **D**) show a *Hox10* triple mutant forelimb and hindlimb, respectively. A control forelimb and hindlimb are shown in (**B** and **E**). (**C** and **F**) show a *Hox11* triple mutant forelimb and hindlimb.

in the axial pattern resulting from mutations in the *Hox10* and *Hox11* paralogous genes, can be explained by a cascade of negative regulatory events among these genes that is analogous to the model first proposed by E. B. Lewis to explain the patterning of the *Drosophila* thoracic and abdominal segments by the *Bithorax* complex (*19*). That is, *Hox10* paralogous genes suppress the formation of thoracic ribs in the lumbar through sacral region. *Hox11* genes, in turn, partially suppress *Hox10* activity in the sacral region, thereby activating the formation of modified ribs that, under the control of *Hox11* genes, fuse and form the sacrum (Fig. 4A). If the ground state for rib formation extends from the head to the tail, then a similar rib-suppressive mechanism, mediated by more anteriorly expressed *Hox* genes, may be used to suppress rib formation in the cervical vertebrae.

It remains to be shown whether the genetic suppressive mechanisms described above are direct or indirect at the molecular level. In more recent evolutionary history, snakes are a dramatic example of vertebrates acquiring, in a sense, a more primitive vertebral body plan through potential changes of *Hox* gene expression pattern (*20*).

The results from this study also extend our understanding of the roles of *Hox* genes in patterning the principal elements of the limbs (Fig. 4, B and C). In the hindlimb, *Hox10* paralogous genes are required to pattern the stylopod, and *Hox11* paralogous genes are required to pattern the zeugopod. In mice that are triple mutant for *Hox10* or *Hox11* paralogous genes, the femur, or the tibia and fibula, respectively, are grossly mispatterned. Fromental-Ramain *et al.* have previously shown that in the absence of *Hoxa13* and *Hoxd13* function (the only *Hox13* paralogs that are expressed in the developing limb bud), the autopods of the forelimb and hindlimb are grossly malformed (*3*). In the forelimb, disruption of the *Hox10* paralogous group affects the formation of the stylopod (that is, the humerus) but to a substantially lesser degree than in the hindlimb. Previous work has shown that mice mutant for both *Hoxa9* and *Hoxd9* exhibit humerus defects very similar to those in the *Hox10* triple mutants (*6*). The *Hox9* paralogous mutations reported, however, had no effect on the patterning of the hindlimbs. This suggests that *Hox9* and *Hox10* paralogous genes may function together in the patterning of the humerus. Taken together with the previous results (*3*, *6*, *21*), the above results complete the assignment of the principal *Hox* genes involved in the patterning of the major limb elements: the stylopod, zeugopod, and autopod.

This study has highlighted the extent of functional redundancy retained among *Hox* paralogous groups as well as the importance of the *AbdB*-group *Hox* genes in patterning the axial and appendicular skeleton. The *Hox1* through *Hox8* paralogous groups are related to individual *Drosophila HomC* homologs. Before vertebrate radiation, the most 5′ *HomC* member, *AbdB*, underwent additional tandem duplications, resulting in the *Hox9* through *Hox13* paralogous groups. These *AbdB*-related genes comprise 16 of the 39 mammalian *Hox* genes. The degree to which expansion of the vertebrate *AbdB* group of genes has contributed to the evolution of the vertebrate body plan is remarkable. The *Hox9* through *Hox13* genes appear to be largely responsible for *Hox* patterning of the limbs as well as the axial skeleton posterior to the thoracic vertebrae. We have shown that the *Hox10* and *Hox11* paralogous genes are global regulators of the lumbosacral region of the axial skeleton and are integral in patterning principal limb elements. Both in the formation of the axial skeleton and in the limbs, all members of a paralogous family that are expressed in a given structure must be disrupted before the full nature of the mutant phenotype is realized. By removing the redundancy in this system, we are beginning to understand the fundamental role these genes play in patterning the vertebrate skeleton.

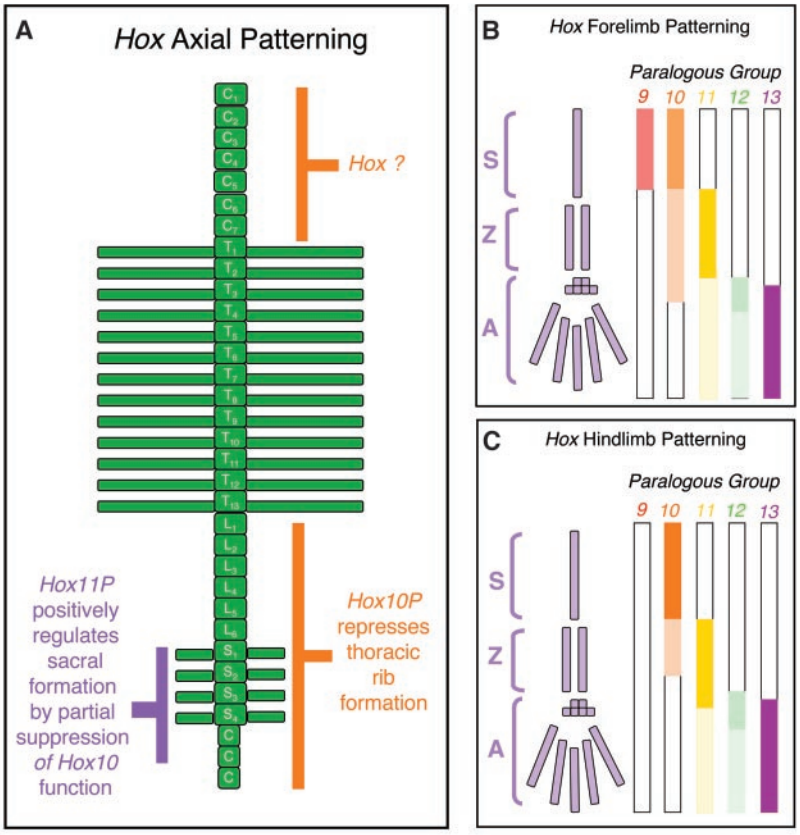

Fig. 4. Schematic representation of *Hox* patterning. (**A**) diagrams the axial phenotypes resulting from loss of *Hox* function. The axial vertebrae are shown as green blocks (for simplicity, only three caudal vertebrae are shown). The function of the *Hox10* paralogous genes is to suppress thoracic development posterior to the 13th thoracic vertebra. In this model, *Hox11* paralogous genes positively regulate the formation of sacral vertebrae by partially suppressing *Hox10* function in the sacral region. In (**B**), functional domains of the *AbdB Hox* genes in forelimb patterning are diagrammed. *Hox9* and *Hox10* paralogs function together to pattern the forelimb stylopod. *Hox10* paralogs also display some phenotype in the zeugopod (lighter orange shading). *Hox11* paralogous genes function mainly in patterning the developing zeugopod, with a lesser contribution to autopod patterning (lighter yellow shading). *Hox13* paralogs function predominantly in the autopod. In the hindlimb (**C**), *Hox9* paralogs do not function. *Hox10* paralogs function predominantly to pattern the stylopod. *Hox11* paralogous genes function mainly in patterning the developing zeugopod, with some contribution to autopod patterning (lighter yellow shading). *Hox13* paralogs function predominantly in the autopod. [Recent work provides evidence that *Hoxd12* can substitute for *Hox13* function in the autopod; patterning therefore is represented with light green shading for *Hox12* function in the autopod (*20*). In (B) and (C), S denotes stylopod, Z zeugopod, and A autopod.]

References and Notes

1. A. C. Burke, C. E. Nelson, B. A. Morgan, C. Tabin, *Development* **121**, 333 (1995).
2. J. L. Nowicki, A. C. Burke, *Development* **127**, 4265 (2000).
3. C. Fromental-Ramain *et al.*, *Development* **122**, 2997 (1996).
4. E. vandenAkker *et al.*, *Development* **128**, 1911 (2001).
5. B. G. Condie, M. R. Capecchi, *Nature* **370**, 304 (1994).
6. C. Fromental-Ramain *et al.*, *Development* **122**, 461 (1996).
7. A. P. Davis, D. P. Witte, H. M. Hsieh-Li, S. S. Potter, M. R. Capecchi, *Nature* **375**, 791 (1995).
8. G. S. B. Horan *et al.*, *Genes Dev.* **9**, 1667 (1995).

9. D. M. Wellik, P. J. Hawkes, M. R. Capecchi, *Genes Dev.* **16**, 1423 (2002).
10. G. M. Wahba, S. L. Hostikka, E. M. Carpenter, *Dev. Biol.* **231**, 87 (2001).
11. D. M. Wellik, M. R. Capecchi, data not shown.
12. S. L. Hostikka, M. R. Capecchi, *Mech. Dev.* **70**, 133 (1998).
13. Y. Herault, J. Beckers, M. Gerard, D. Duboule, *Dev. Biol.* **208**, 157 (1999).
14. P. Dolle, J. C. Izpisua-Belmonte, H. Falkenstein, A. Renucci, D. Duboule, *Nature* **342**, 767 (1989).
15. P. Dolle, J. C. Izpisua-Belmonte, J. M. Brown, C. Tickle, D. Duboule, *Genes Dev.* **5**, 1767 (1991).
16. B. Favier *et al.*, *Development* **122**, 449 (1996).
17. M. Suzuki, A. Kuroiwa, *Mech. Dev.* **118**, 241 (2002).
18. M. Hildebrand, *Analysis of Vertebrate Structure* (Wiley, New York, ed. 4, 1995).
19. E. B. Lewis, *Nature* **276**, 565 (1978).
20. M. J. Cohn, C. Tickle, *Nature* **399**, 474 (1999).
21. M. Kmita, B. Tarchini, D. Duboule, Y. Harault, *Development* **129**, 5521 (2002).
22. We are indebted to S. L. Hostikka for preparation of the *Hoxc10* and *Hoxc11* mutant mice, and we thank J. F. Fallon, S. Sakonju, and B. W. Bisgrove for discussions of these data before publication.

Supporting Online Material
www.sciencemag.org/cgi/content/full/301/5631/363/DC1
SOM Text
References

14 April 2003; accepted 9 June 2003

DNA: A Programmable Force Sensor

Christian Albrecht,[1] Kerstin Blank,[1] Mio Lalic-Mülthaler,[1] Siegfried Hirler,[1] Thao Mai,[1] Ilka Gilbert,[1] Susanne Schiffmann,[1] Tom Bayer,[1] Hauke Clausen-Schaumann,[1]* Hermann E. Gaub[2]

Direct quantification of biomolecular interaction by single-molecule force spectroscopy has evolved into a powerful tool for materials and life sciences. We introduce an approach in which the unbinding forces required to break intermolecular bonds are measured in a differential format by comparison with a known reference bond (here, a short DNA duplex). In addition to a marked increase in sensitivity and force resolution, which enabled us to resolve single–base pair mismatches, this concept allows for highly specific parallel assays. This option was exploited to overcome cross-reactions of antibodies in a protein biochip application.

Within the past decade, a variety of experimental tools based on applying and measuring piconewton forces between single molecules have been developed and have contributed to a better understanding of the mechanics of biomolecules and molecular bonds (*1–4*). Force measurements reveal detailed insights into binding-potential landscapes and into functional aspects of the molecules under investigation, and as a result, force has become a new structural and functional parameter in materials and life sciences. Receptor-ligand pairs (*5–8*), protein and nucleic acid structures (*9–15*), and even covalent bonds (*16*) have been investigated, and it has become evident that biomolecular processes are governed by piconewton forces. However, two major bottlenecks have hindered the widespread use of single-molecule mechanics: sizable instrumental effort and limited force resolution. To our knowledge, no single–base pair mismatch detection by single-molecule force measurements has been reported, despite numerous efforts. The best resolution to date has been 10 base pairs (bp), obtained by shearing and unzipping short oligomers by atomic force micoscopy (AFM) (*17*, *18*).

In conventional single-molecule force spectroscopy, inter- or intramolecular forces are exerted and measured with microscopic force sensors like AFM cantilevers or beads in optical or magnetic traps (*19*, *20*). With state-of-the-art instrumentation, the force resolution is limited only by thermal fluctuations that are detected by the force sensor. Arguments based on the fluctuation-dissipation theorem predict that a reduction of the sensor size should improve the signal-to-noise ratio (*21*). This has been verified in experimental studies using a new generation of small AFM cantilevers (*22*). The logical extrapolation is to replace the cantilever by a single elastic molecule. To increase the precision of the assay even further, we chose a differential measurement format, where rupture forces of two molecular complexes are directly compared with each other. This differential format offers several advantages. Because of the high symmetry of the assay, most external disturbances cancel out (*23*). In addition, for most applications, a precise measure of the difference is more valuable than two absolute values with their respective error bars, such as the ranking of binders or a single–base pair mismatch detection in a DNA sequence.

In our setup (Fig. 1), the cantilever spring was replaced by a polymeric anchor and a known molecular bond (reference bond) carrying a fluorescence label. The molecular bond under investigation was directly compared to this reference bond, which served as a molecular force standard. During separation of the two surfaces, the polymeric anchor was stretched, and the force acting along the molecular chain consisting of the sample and labeled reference complex built up gradually, until the weaker of the two bonds ruptured. The difference in the stability of the two bonds breaks the symmetry in this experiment. As a result, there is a higher probability that the fluorescence label will end up on the side of the stronger bond rather than on the side of the weaker bond. This process can be seen as a 1-bit analog-to-digital conversion broadened by thermal fluctuations (*24*). Many single-molecule force measurements can be performed simultaneously, using two congruent chip surfaces and different spots containing the molecules of interest. Counting the labels on each side, for instance, by single-molecule optics, provides a quantitative measure for the differences between the distributions of the bond rupture probabilities of the two molecular complexes. It is equivalent to measuring the fluorescence intensities, which are proportional to the densities of the fluorescence labels (*25*). Although a large number of molecules are probed simultaneously, the actual force measurement is still performed at the single-molecule level, because each sample bond is probed individually by a single reference bond.

Figure 1B illustrates the setup schematically. The rupture forces of two DNA strands with different hybridization lengths (a 20-bp duplex and a 25-bp duplex) are directly compared. Both oligonucleotides are bridged with a conjugated 65-base oligonucleotide, carrying a terminal Cy5 fluorescent label. The resulting 20-bp duplex is coupled to an activated glass surface, and the 25-bp duplex to a soft polydimethylsiloxane (PDMS) stamp (*26–28*), both by means of polyethylene glycol (PEG) spacers. Figure 1C shows fluorescence images of the glass surface containing the capture oligonucleotide and the labeled sample oligonucleotide before the two surfaces were brought into contact and separated again, and both glass (bottom) and PDMS (top) after the separation of the two surfaces. Because the PDMS stamp has a grid pattern of trenches to ease the water flux at the surface during separation, the transferred labels form a checkerboard pattern on the PDMS. No transfer occurred in the trenches, so that here the initial label density was maintained on the glass surface, whereas in the contact areas (squares), labels were transferred from the glass to the PDMS side.

[1]Nanotype GmbH, Lochhamer Schlag 12, 82166 Gräfelfing, Germany. [2]Lehrstuhl für Angewandte Physik and Center for Nano-Science, Amalienstrasse 54, 80799 München, Germany.

*To whom correspondence should be addressed. E-mail: hauke.clausen-schaumann@nanotype.de